

1 **JSC-Rocknest: A large-scale Mojave Mars Simulant (MMS) based soil simulant for in-situ**
2 **resource utilization water-extraction studies**

3 Clark, J.V.^{a*}, Archer, P.D.^b, Gruener, J.E.^c, Ming, D.W.^c, Tu, V.M.^b, Niles, P.B.^c, Mertzman,
4 S.A.^d

5 ^a GeoControls Systems, Inc – Jacobs JETS Contract at NASA Johnson Space Center, 2101
6 NASA Pkwy, Houston, TX 77058, USA. joanna.hogancamp@nasa.gov, 281-244-7442

7 ^b Jacobs JETS Contract at NASA Johnson Space Center, 2101 NASA Pkwy, Houston, TX
8 77058, USA.

9 ^c NASA Johnson Space Center, 2101 NASA Pkwy, Houston, TX 77058, USA.

10 ^d Department of Earth and Environmental, Franklin & Marshall College, Lancaster, PA 17604,
11 USA.

12 *Corresponding author

13

14

15

16

17

18

19 Keywords: Simulant, Mars, In-situ resource utilization, evolved gas analysis, Rocknest

20 **Abstract**

21 The Johnson Space Center-Rocknest (JSC-RN) simulant was developed in response to a
22 need by NASA's Advanced Exploration Systems (AES) In-Situ Resource Utilization (ISRU)
23 project for a simulant to be used in component and system testing for water extraction from Mars
24 regolith. JSC-RN was designed to be chemically and mineralogically similar to material from the
25 aeolian sand shadow named Rocknest in Gale Crater, particularly the 1-3 wt.% low temperature
26 (<450 °C) water release as measured by the Sample Analysis at Mars (SAM) instrument on the
27 *Curiosity* rover. Sodium perchlorate, goethite, pyrite, ferric sulfate, regular and high capacity
28 granular ferric oxide, and forsterite were added to a Mojave Mars Simulant (MMS) base in order
29 to match the mineralogy, evolved gases, and elemental chemistry of Rocknest. Mineral and rock
30 components were sent to the United States Geological Survey (USGS) in Denver for mixing.
31 Approximately 800 kg of JSC-RN was sent back to NASA in 5 gallon buckets, which were
32 subsampled and characterized. All samples of the USGS-produced simulants had similar evolved
33 gas profiles as a small prototype batch of JSC-RN made in JSC laboratories, with the exception
34 of HCl, and were similar in terms of mineralogy and total chemistry. Also, all JSC-RN
35 subsamples were homogenous and had similar mineralogy, total chemistry, and low-temperature
36 evolved gas profiles as the Rocknest aeolian sand shadow examined with *Curiosity's* instrument
37 suite on Mars. In particular, the low temperature water releases were similar and the amount of
38 water evolved from JSC-RN at <450 °C was similar to the water content of Rocknest based on
39 SAM water peak integrations. Overall, JSC-RN is ideally suited for ISRU studies of water
40 extraction of global martian soil due to its excellent agreement with measured properties of
41 martian soils and its proven feasibility for large-scale production.

42

43 **1. Introduction**

44 Martian soil simulants are materials that are mineralogically, chemically, and/or
45 geotechnically similar to martian regolith, and can be used for multiple purposes such as
46 scientific research, education, mission development, and to test and develop in-situ resource
47 utilization (ISRU) technologies. The fidelity of a simulant depends on the application it is being
48 used for. For example, the testing of rover wheels would require a simulant that closely matches
49 the geotechnical properties of martian surface materials. Martian soil simulants are of particular
50 interest to ISRU because of the abundance of soil (defined here as unconsolidated material) on
51 the surface of Mars and the ease with which it can be excavated from the surface compared to
52 solid rock. The most well characterized soil to date was called Rocknest and was analyzed by the
53 Mars Science Laboratory (MSL) *Curiosity* rover's instrument suite. Rocknest is an ideal basis for
54 a new martian soil simulant because it has been extensively characterized and has been
55 interpreted to represent local soil and possibly global martian soil (Blake et al., 2013; Bish et al.,
56 2013; Archer et al., 2014).

57 Johnson Space Center-Rocknest (JSC-RN) is a new simulant that was specifically designed
58 to be produced in large quantities and used by the National Aeronautical and Space
59 Administration (NASA) Advanced Exploration Systems (AES) ISRU project in component and
60 system testing for water extraction from martian soil. Water can be extracted from
61 unconsolidated material through heating, where adsorbed and structural water are thermally
62 removed from regolith materials. The water can then be condensed and purified for use as
63 drinking water or split by electrolysis into hydrogen and oxygen for use as propellant for
64 spacecraft or as a source of breathable O₂. As such, the focus of JSC-RN was to replicate the
65 evolved gas profiles, especially the low temperature (<450 °C) water release, detected in

66 Rocknest by the Sample Analysis at Mars (SAM) instrument on the *Curiosity* rover. It was
67 essential that JSC-RN be cost-effective and composed of materials that could be purchased
68 commercially (i.e., not synthesized in the lab) because many ISRU system and component tests
69 require hundreds of kilograms of simulant. Here, we describe the development and
70 characterization of JSC-RN, which is based on the evolved gases, mineralogy, and total
71 chemistry of the Rocknest aeolian sand shadow.

72 1.1 Mineralogical, geochemical, and physical properties of martian soils

73 1.1.1 *In-situ* analysis of Rocknest

74 The first sample scooped by the MSL *Curiosity* rover was named Rocknest, and was
75 collected on top of the Bradbury group, which underlies the Mount Sharp group in northern Gale
76 Crater (Sutter et al., 2017). It was sampled from an inactive, dust-covered sand shadow that was
77 interpreted to be deposited by northerly winds on the leeward side of an obstacle (Blake et al.,
78 2013).

79 Five samples were scooped from the Rocknest sand shadow and individually delivered to
80 the Sample Acquisition, Sample Processing and Handling–Collection and Handling for In situ
81 Martian Rock Analysis (SA/SPaH-CHIMRA) instrument, where they were sieved to a grain size
82 of <150 μm (Blake et al., 2013). Approximately 40-50 mg portions of scoops 3 and 4 were
83 delivered to the Chemistry and Mineralogy (CheMin) X-ray diffractometer (XRD) and scoop 5
84 was delivered to both SAM and CheMin.

85 The <150 μm size fraction of Rocknest was delivered to the SAM oven for heating from 40
86 to 870 $^{\circ}\text{C}$ at a heating rate of approximately 35 $^{\circ}\text{C}/\text{min}$ (Sutter et al., 2017). As the sample was
87 heated, volatile-bearing phases thermally decomposed and the evolved gases (e.g., O_2 , H_2O , SO_2 ,

88 HCl) were then sent to a quadrupole mass spectrometer (QMS), tunable laser spectrometer
89 (TLS), or gas chromatograph (GC) using a helium carrier gas (~0.8 sccm) (Mahaffy et al., 2012;
90 Webster et al., 2013; Freissinet et al., 2015).

91 Alpha Proton X-ray Spectrometer (APXS) bulk chemical analysis was performed on
92 <150 µm sieved material that was delivered to the observation tray on top of the rover. APXS
93 analysis was also done on a wheel scuff in the Rocknest sand shadow called “Portage”, which
94 was un-sieved. Chemical analyses of sieved and un-sieved portions of the Rocknest sand shadow
95 were largely similar (Blake et al., 2013; Bish et al., 2013).

96 1.1.2 Mineralogical properties of Rocknest and global martian soils

97 CheMin XRD analyses of Rocknest showed that it was mineralogically similar to martian
98 basalts as well as basalts found in martian meteorites (Blake et al., 2013). The crystalline
99 component contained plagioclase feldspar, olivine, and pyroxene (Table 1; Bish et al., 2013;
100 Achilles et al., 2017). The chemical composition of olivine was estimated using refined unit-cell
101 parameters in Rietveld refinements and showed it was consistent with the Mg-rich endmember
102 forsterite (Morrison et al., 2018a; 2018b; Bish et al., 2013). CheMin did not detect perchlorates,
103 halides, carbonates, phosphates, or sulfates in the crystalline portion; therefore, if these phases
104 were present, they were non-crystalline or below the CheMin detection limit of 1-2 wt.% (Bish et
105 al., 2013). Rocknest also contained a large (~35 wt. %) X-ray amorphous component consistent
106 with basaltic glass, allophane, poorly crystalline sulfate, and nanophase iron oxides such as
107 ferrihydrite (Bish et al., 2013; Sutter et al., 2017; Achilles et al., 2017). The amorphous
108 component was rich in Si, Fe, and S (Achilles et al., 2017).

109 Prior to MSL, observations by several landers, rovers, and orbiters categorized martian soils
110 as either “bright dust” or “dark soil” and determined that they were mineralogically and
111 chemically uniform across the martian surface (Yen et al., 2005). Bright dust exists as a ~1 mm
112 thick surface layer and the particle size has not been determined with certainty due to the
113 resolution of *in-situ* imagers (Yen et al., 2005; Ming & Morris, 2017). Dark soils are located
114 beneath the bright dust layer and have grain sizes up to 100 μm (Yen et al., 2005). *In-situ*
115 analyses by *Viking* I and II, Mars *Pathfinder*, the Mars Exploration Rovers (MER) *Spirit* and
116 *Opportunity*, and *Phoenix* used instruments including the Miniature Thermal Emission
117 Spectrometer (Mini-TES), multispectral imagers, and Mössbauer spectrometer to estimate
118 surface and subsurface mineralogy and chemistry of martian soils (Yen et al., 2005, and
119 references therein). Additionally, orbiter-based spectrometers provided information on the global
120 distribution of soils and their estimated mineralogies; however, due to instrument limitations
121 (e.g., could not distinguish between some spectrally similar phases) these data were not as
122 definitive and robust as those from the CheMin XRD on *Curiosity*. Multispectral imagers on the
123 MER and *Pathfinder* rovers showed that the bright soils were dominated by nanophase iron
124 oxides and the dark soils contained altered iron-bearing minerals and ferrous iron-bearing
125 silicates (Yen et al., 2005). Nanophase iron oxides, such as palagonite or ferrihydrite, have been
126 detected in other spectrally bright regions of Mars including Olympus Mons and Amazonis
127 Planitia (Morris et al., 2000). Local bright soil deposits in Gusev Crater and Meridiani Planum
128 had Mini-TES signatures similar to Mars Global Surveyor TES signatures of global average
129 martian dust, suggesting that bright dust is globally distributed across the martian surface (Yen et
130 al., 2005). *In-situ* and Mars Global Surveyor TES results suggested that global dust is composed
131 of framework silicates, olivine, pyroxene, amorphous material, hematite, and magnetite

132 (Hamilton et al., 2005). The iron-mineralogy and spectral characteristics of dark soils at Gusev
 133 Crater and Meridiani Planum were similar, suggesting that dark soils may also be globally
 134 distributed, or at least are derived from sources of similar composition (Yen et al., 2005).

135
 136 Table 1. Quantitative mineralogy (wt.%) of MGS-1, MMS, and the USGS produced JSC-RN
 137 simulant compared to Rocknest analyzed by CheMin. Rocknest mineralogy was based on
 138 Rietveld refinement and FULLPAT analyses of CheMin data (Achilles et al., 2017). The MMS
 139 mineralogy is based on a 35 wt.% < 2 mm/65 wt.% dust mixture analyzed at JSC. The JSC-RN
 140 mineralogy was based on the average quantitative mineralogy of three subsamples from USGS
 141 prepared mixtures, shown with standard deviations. MGS-1 mineralogy is based on the recipe
 142 listed in Cannon et al., (2019). Mineralogy of JSC Mars-1 was not reported. n.d. = not detected.

Mineral	Rocknest Crystalline + Amorphous	MGS-1	MMS (measured at JSC)	JSC-RN average
Plagioclase	26.3 ± 7	27.1	60.4	42.9 ± 0.5
Olivine	13.3 ± 4	13.7	n.d.	11.7 ± 0.8
Pyroxene	19.7 ± 8.5	20.3	12.3	11.0 ± 0.5
Magnetite	1.8 ± 3	1.9	n.d.	n.d.
Anhydrite	0.9 ± 2	0.9	n.d.	n.d.
Hematite	1.0 ± 1	1.1	1.1	1.7 ± 0.4
Quartz	0.8 ± 2	n.d.	0.6	2.3 ± 2.8
Calcite	n.d.	n.d.	1.0	1.5 ± 0.3
Ilmenite	0.9 ± 3	n.d.	2.2	1.0 ± 0.2
K-feldspar	n.d.	n.d.	2.2	2.3 ± 0.6
Analcime	n.d.	n.d.	1.3	1.0 ± 0.1
Goethite	n.d.	n.d.	n.d.	1.7 ± 0.3
Pyrite	n.d.	n.d.	n.d.	0.6 ± 0.0
Ferric sulfate	n.d.	n.d.	n.d.	0.3 ± 0.1
Amorphous	35 ± 15	35	3.1	-
Amorphous + smectite	-	-	18.7	20.4 ± 1.3

143

144 1.1.3 Geochemical properties of Rocknest and martian soils

145 APXS analyses of the Rocknest sand shadow revealed basaltic chemistry dominated by SiO₂
146 and FeO_{total} (Table 2), and was similar to soils analyzed across Mars (Bish et al., 2013; Blake et
147 al., 2013; Yen et al., 2005). The bulk chemistry of Rocknest as detected by APXS was within
148 two standard deviations of MER APXS analyses of basaltic soils at the Gusev Crater and
149 Meridiani Planum landing sites (Blake et al., 2013). Rocknest contained slightly lower SiO₂
150 (42.97 wt.%) than Gusev Crater (46.1 wt.%) and Meridiani Planum (45.7 wt.%). Rocknest also
151 contained slightly higher iron (19.18 wt.%) than Gusev Crater (16.3 wt.%) and Meridiani
152 Planum (18.8 wt. %) (Blake et al., 2013). The general similarity of the chemical compositions
153 between Rocknest and bright soils in Gusev Crater and Meridiani Planum indicates that martian
154 soils possess a dust component that is globally distributed across Mars as well as a local
155 component that is similar across many regions on Mars (Blake et al., 2013).

156

157

158

159

160

161

162

163

164 Table 2. Alpha Proton X-ray Spectrometer (APXS) chemical composition data from Rocknest
 165 bulk material measured from disturbed soil (Achilles et al., 2017) compared to JSC-RN and other
 166 martian simulants. The chemistry of JSC-RN is based on the average of 21 subsamples of large-
 167 scale batches of JSC-RN mixed by the USGS, and is shown with standard deviations.

Oxide	Rocknest bulk, wt. %	JSC Mars-1 ¹	MGS-1 ²	MMS ³	JSC-RN (small prototype), wt.%	JSC-RN (USGS, averaged), wt.%
SiO ₂	42.97	43.5	47.2	49.8	45.96	45.82 ± 0.18
TiO ₂	1.19	3.8	0.4	1.1	1.07	1.06 ± 0.02
Al ₂ O ₃	9.37	23.3	11.6	17.2	13.73	13.66 ± 0.09
FeO _T	19.18	15.6	17.5	11.0	17.76	17.71 ± 0.19
MnO	0.42	0.3	0.1	0.2	0.18	0.18 ± 0.01
MgO	8.69	3.4	9.9	6.1	9.38	9.51 ± 0.06
CaO	7.26	6.2	5.6	10.5	7.61	7.97 ± 0.03
Na ₂ O	2.70	2.4	2.8	3.3	3.06	3.05 ± 0.02
K ₂ O	0.49	0.6	0.5	0.5	0.54	0.54 ± 0.01
P ₂ O ₅	0.95	0.9	0.1	0.2	0.16	0.16 ± 0.00
Cr ₂ O ₃	0.49	-	0.1	0.1	0.05	0.06 ± 0.00
Cl	0.69	-	-	-	0.24	0.43 ± 0.13
%SO ₃	5.47	-	4.3	0.1	1.00	1.77 ± 0.27
Total	99.87	100.0	100	100	99.45	99.65 ± 0.21

168

169 1.1.4 Volatile properties of Rocknest and martian soils

170 H₂O evolved during the heating of the Rocknest soil sample was attributed to phases in
 171 both the crystalline and amorphous components, and was similar to the water content of other
 172 martian soils (Archer et al., 2014; Sutter et al., 2017). Most (~80 %) of the water in Rocknest
 173 was evolved <450 °C and was characterized by a broad release that peaked around 280 °C and
 174 tapered off around 450 °C (Figure 1; Archer et al., 2014). The broad low temperature water
 175 release likely had contributions from multiple sources, including adsorbed water from high
 176 surface area nanophase iron oxides in the amorphous component (Archer et al., 2014; Achilles et

¹ Allen et al., 1998

² Cannon et al., 2019

³ Peters et al., 2008

177 al., 2017). Structural H₂O, structural OH, or water inclusions could also have contributed to the
178 observed water release (Archer et al., 2014). Evolved water content in the Rocknest soil sample
179 (2.0 ± 1.3 wt.%; Archer et al., 2013; Table 3) was similar to water content in soils analyzed in
180 Chryse Planitia and Utopia Planitia by the *Viking* landers (~1 %; Biemann et al., 1977).

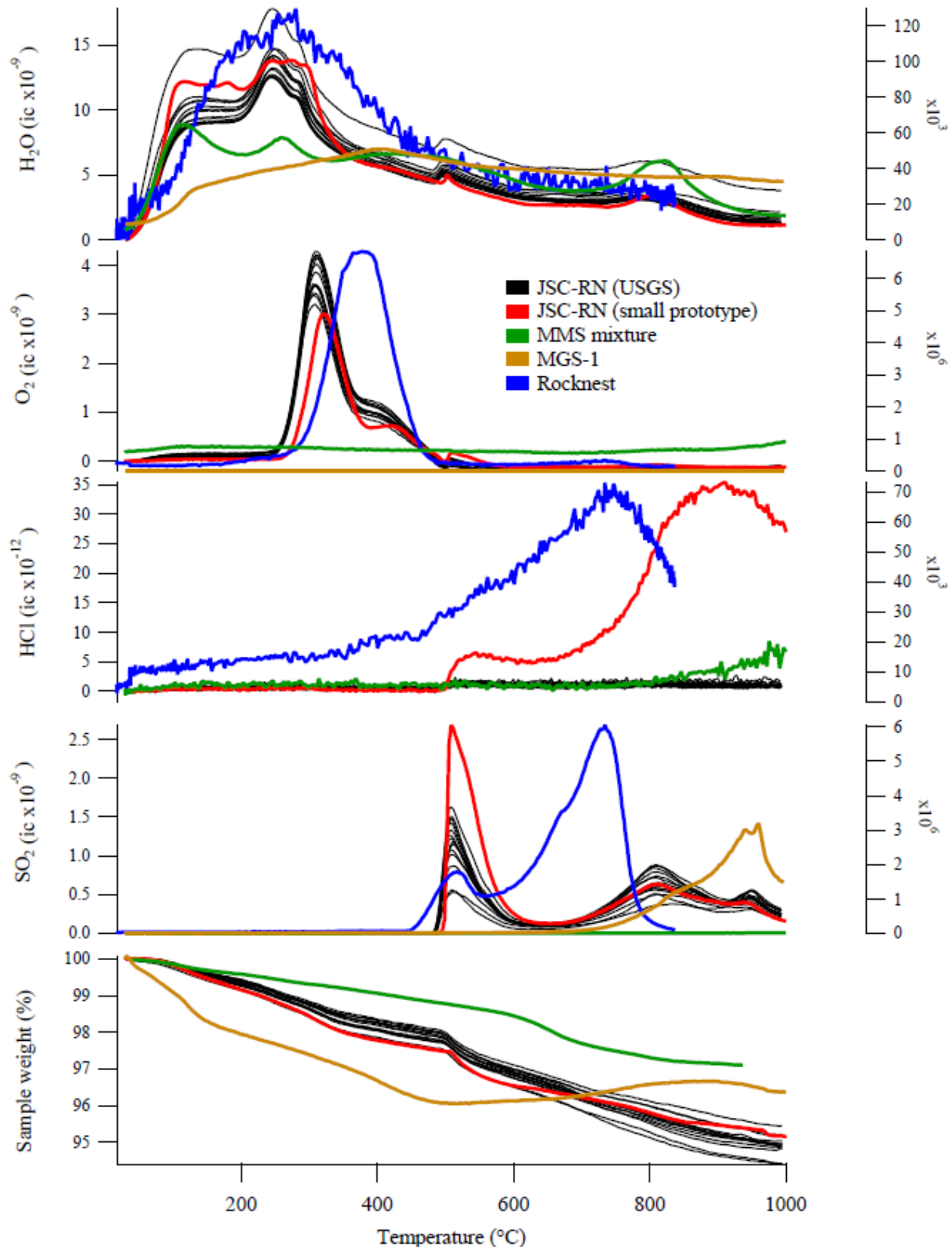
181 Evolved O₂ from Rocknest peaked ~380 °C and was likely caused by the thermal
182 decomposition of an oxychlorine (i.e., perchlorate or chlorate) (Figure 1; Archer et al., 2014;
183 Sutter et al., 2017; Hogancamp et al., 2018). The presence of oxychlorines was supported by the
184 simultaneous release of mid temperature O₂ and chlorinated hydrocarbons (Archer et al., 2014).
185 Thermal decomposition of perchlorates or chlorates (with the exception of Mg and Fe
186 oxychlorines) produced chlorides, which then reacted with water and other minerals (e.g.,
187 sulfates) in the sample to evolve high temperature (>600 °C) HCl (Sutter et al., 2017; Clark et
188 al., 2020). The HCl release from Rocknest started at ~475 °C and steadily increased with a peak
189 at ~750 °C (Figure 1; Archer et al., 2014; Sutter et al., 2017), which is characteristic of
190 perchlorate/water-producing phase mixtures run in the laboratory under SAM-like conditions
191 (Clark et al., 2020). Oxychlorines have also been detected at 0.4-0.6 % by the Thermal and
192 Evolved Gas Analyzer (TEGA) instrument and the Wet Chemistry Lab (WCL) on the *Phoenix*
193 lander and have been suggested to be globally distributed in martian regolith (Hecht et al., 2009).

194 Evolved SO₂ peaks at ~515 °C and ~730 °C in Rocknest were attributed to the presence
195 of sulfates, sulfites, and/or sulfides (McAdam et al., 2014). The SO₂ peak at ~515 °C was
196 attributed to the oxidation of a sulfide such as pyrite or pyrrhotite because an increase in evolved
197 SO₂ coincided with a decrease in O₂ (Figure 1; McAdam et al., 2014). The SO₂ peak at ~730 °C
198 could be caused by the thermal decomposition of calcium sulfite, which can form by the reaction
199 of CaCl₂, SO₂, and H₂O (McAdam et al., 2014). It could also be caused by the thermal

200 decomposition of iron sulfate or from SO_4^{2-} adsorbed on high surface area particles (McAdam et
 201 al., 2014). Sulfates are believed to be globally distributed across Mars but have not been detected
 202 in soils by evolved gas analysis prior to the Rocknest soil sample. Sulfates were likely present at
 203 the *Phoenix* landing site because they are globally distributed and S and Cl correlate in martian
 204 global dust and soils (Golden et al., 2009). SO_2 peaks <1000 °C were not detected by TEGA at
 205 the *Phoenix* landing site, suggesting that Mg- and Fe sulfates were not present (Golden et al.,
 206 2009). If sulfates were present at the *Phoenix* landing site, they may have been in the form of Ca-
 207 or Na sulfate because these phases thermally decompose above the temperature range of TEGA
 208 and both cations were detected by the WCL (Golden et al., 2009).

209
 210 Table 3. Weight percentages of major and some minor volatiles, pertinent to this work, that were
 211 released from the Rocknest soil sample during heating to ~ 870 °C. SO_3 and ClO_4 abundances
 212 were calculated from SAM SO_2 and O_2 releases, respectively. Ranges are based on the average
 213 values from four SAM analyses of Rocknest. (Archer et al., 2014)

Volatile	Abundance (wt.%)
H_2O	1.6-2.4
SO_3	0.5-3.5
ClO_4	0.3-0.5
CO_2	0.7-1.0



215 Figure 1. Evolved H₂O, O₂, HCl, and SO₂ from laboratory analyses of a small prototype mixture
216 of JSC-RN prepared in the JSC laboratory, 13 subsamples of JSC-RN mixed in large-scale
217 quantities at the USGS, a 35 wt.% <2 mm/65 wt.% dust MMS mixture, MGS-1, and Rocknest
218 analyzed by SAM on the *Curiosity* rover. Laboratory data are shown on the primary y-axis and
219 SAM data are shown on the secondary y-axis. Thermal gravimetric (TG) data are shown for the
220 small-scale and large-scale versions of JSC-RN, MMS, and MGS-1. EGA data were not
221 available for JSC Mars-1 and HCl data were not available for MGS-1.

222

223 1.2 Previous martian soil simulants

224 Several martian soil simulants exist, including Johnson Space Center Mars-1 (JSC Mars-1),
225 Mojave Mars Simulant (MMS), and Mars Global Simulant (MGS-1). JSC Mars-1 consists of
226 weathered volcanic ash that was spectrally similar to bright dust on the martian surface, and was
227 developed primarily for use in science research, engineering studies, and education. JSC Mars-1
228 was sourced from meteorically altered basaltic material from late a Pleistocene cinder cone on
229 the flank of Mauna Kea volcano in Hawaii (Allen et al., 1998). Meteoric weathering of this
230 volcanic material produced a suite of minerals similar to the bright regions of Mars based on
231 orbital spectral data (Evans and Adams, 1979; Morris et al., 1993; Allen et al., 1998). JSC Mars-
232 1 primarily consists of “finely crystallized and glassy particles of a volcanic rock known as
233 ‘hawaiite’ (Allen et al., 1998, pp.406). The bulk quantitative mineralogy of JSC Mars-1 contains
234 calcium feldspar, minor magnetite, and a large amorphous component rich in ferric oxide (Allen
235 et al., 1998). The total chemistry of JSC Mars-1 is dominated by SiO₂, Al₂O₃, and FeO_{total} (Allen
236 et al., 1998; Table 2). JSC Mars-1 does not replicate the volatile properties of well-characterized
237 martian soils; it lost 7.8 wt.% and 21.1 wt.% when heated to 100 °C and 600 °C, respectively,

238 primarily due to water adsorbed on mineral surfaces and contained within glass particles (Allen
239 et al., 1998). The water content of JSC Mars-1 is far greater than water content of martian soils
240 measured *in-situ* by TEGA on the *Phoenix* lander or the SAM instrument on the *Curiosity* rover
241 (Leshin et al., 2013; Smith et al., 2009).

242 MMS is mineralogically and chemically similar to igneous rocks on Mars and their
243 weathering products, and was developed based on newly acquired physical and chemical data
244 from martian soils. While JSC Mars-1 relied upon orbital observations, MMS was developed
245 using data from *in-situ* analyses by the *Viking* landers, Mars *Pathfinder*, and MER *Spirit* in
246 addition to orbital data (Peters et al., 2008). MMS was sourced by the Jet Propulsion Laboratory
247 (JPL) for testing instruments and sampling systems for the *Phoenix* and MSL missions. MMS is
248 crushed Saddleback Basalt sieved to >2 mm granules, <2 mm sand, and dust (Peters et al., 2008).
249 The Saddleback Basalt was sourced from an early Miocene outcrop in the western Mojave
250 Desert near Boron, California and was commercially mined by Carlton Global Resources (CGR)
251 (Peters et al., 2008). Peters et al. (2008) reported that the mineralogy of MMS was dominated by
252 plagioclase feldspar, pyroxene, olivine, and magnetite and was chemically similar to martian
253 basalts. The bulk mineralogy of MMS sent to JSC from JPL did not contain olivine or magnetite,
254 as reported in Peters et al., (2008). Additionally, Peters et al. (2008) did not report any
255 phyllosilicates or calcite, which were detected at about 15.6 wt.% and 1.0 wt.%, respectively, in
256 the MMS mixture sent to JSC. It is possible that the batches of MMS sent to JSC were sourced
257 from a chemically altered area of the Saddleback Basalt, explaining the presence of
258 phyllosilicates and calcite. Although MMS broadly mimics the mineralogy and chemistry of
259 martian regolith, it does not replicate the evolved gases (e.g., O₂, H₂O, SO₂, HCl) from martian

260 soils analyzed by either TEGA or SAM (Figure 1). Specifically, MMS lost ~1 wt.% water at 450
261 °C (Figure 1), whereas Rocknest contained 2.0 ± 1.3 wt.% water (Archer et al., 2014).

262 The University of Central Florida developed the Mars Global Simulant-1 (MGS-1) in order
263 to more precisely replicate martian global basaltic regolith based on newly available physical and
264 chemical data from the Rocknest soil sample analyzed by the *Curiosity* rover (Cannon et al.,
265 2019). MGS-1 was developed as a mineralogical standard for basaltic soils on Mars and consists
266 of 13 components (Cannon et al., 2019; Table 1). Mineral-based simulants like MGS-1 are
267 created by physically mixing individual minerals rather than crushing a rock or sourcing a
268 natural soil. Mineral-based simulants are ideal for experiments where mineralogical fidelity to
269 martian soil is of utmost importance, such as mineral alteration studies. Crushed rock-based
270 simulants are preferred for geotechnical tests (e.g., rover wheel testing) over mineral-based
271 simulants because they more closely approximate the physical properties of natural soils (Peters
272 et al., 2008). Additionally, MGS-1 does not accurately capture the low temperature evolved
273 gases of the Rocknest soil sample, particularly the low temperature water. MGS-1 lost ~3.7 wt.%
274 water <450 °C with a water release peak ~400 °C, whereas Rocknest contained 2.0 ± 1.3 wt.%
275 (Archer et al., 2014) and evolved a water release peak at ~280 °C (Figure 1).

276 Here, we describe the development and characterization of a new crushed rock-based martian
277 soil simulant, Johnson Space Center-Rocknest (JSC-RN), which was specifically designed to be
278 produced in large quantities and used by the NASA AES ISRU project in component and system
279 testing for water extraction from martian soil. JSC-RN uses MMS as a base but contains
280 additives in order to better approximate the chemical, mineralogical, and volatile properties of
281 martian soils. Unlike previous simulants, the primary focus of JSC-RN was to simulate the low

282 temperature evolved gases, particularly the 1-3 wt.% low temperature (<450 °C) water release as
283 measured by the SAM instrument on the *Curiosity* rover (Leshin et al., 2013).

284

285 **2. Methods**

286 2.1 Thermal and evolved gas analysis

287 Powdered samples (e.g., individual minerals, simulant mixtures) were analyzed on a
288 Setaram Labsys EVO simultaneous thermal gravimeter (TG)/differential scanning calorimeter
289 (DSC) connected to a ThermoStar quadrupole mass spectrometer for evolved gas analysis
290 (EGA). This technique matches the EGA capability of the SAM instrument on the *Curiosity*
291 rover, adding TG and DSC capabilities to provide a more complete understanding of reactions
292 and phase transitions in the laboratory samples. TG measures sample weight loss as a sample is
293 heated, and was used to determine the amount of water evolved from the sample at low
294 temperatures (<450 °C). DSC measures exothermic and endothermic phase transitions and
295 chemical reactions as a sample is heated. EGA is used to measure and quantify the gases released
296 from the sample during pyrolysis. Samples (~10-50 mg) were loaded into an alumina ceramic
297 crucible and placed inside the Labsys furnace alongside an identical empty reference crucible.
298 The system was purged with He carrier gas at a flow rate of 10 sccm and pressure of 30 mbar,
299 similar to the carrier gas and pressure conditions on the SAM instrument. The sample crucible
300 and the empty crucible were heated from room temperature to 1000 °C at a heating rate of 35
301 °C/min.

302

303

304 2.2 X-ray diffraction

305 Powdered samples were individually analyzed for qualitative mineralogy using a
306 PANalytical X'Pert Pro MPD X-ray diffraction instrument with an X'celerator detector and Co
307 $K\alpha$ radiation. Data were collected under ambient conditions at a step size of 0.02° per minute
308 from 2° to 80° 2θ at 40 mA and 45kV. Minerals were identified using HighScore software
309 equipped with the International Center for Diffraction Data (ICDD) database and the
310 Crystallography Open Database (COD).

311 Select samples were analyzed for quantitative mineralogy using the above methods and
312 Reitveld refinement in HighScore and MDI JADE software. The select samples were spiked
313 with a National Institute of Standards and Technology (NIST) corundum (Al_2O_3) standard in
314 order to quantify mineral and X-ray amorphous abundances (Bish and Howard, 1988).
315 Novaculite and NIST lanthanum hexaboride standards were used to characterize the instrument's
316 2θ alignment and line broadening function, respectively.

317

318 2.3 X-ray fluorescence

319 Powdered samples were analyzed for bulk chemistry using a Malvern PANalytical Zetium X-
320 ray Fluorescence (XRF) vacuum spectrometer. ~1 gram of each sample was placed in a muffle
321 furnace at $950^\circ C$ for 1.5 hours. 0.4000 g of each post-loss on ignition (LOI) sample was mixed
322 with 3.6000 g of 4-9s pure lithium tetraborate, placed in a platinum crucible, and heated with a
323 meeker burner until completely melted. The melt was mixed three times during the heating stage,
324 transferred to a platinum casting dish, and quenched to form a glass disk for XRF analysis
325 including SiO_2 , TiO_2 , Al_2O_3 , Fe_2O_3 total, MnO, MgO, CaO, Na_2O , K_2O , and P_2O_5 . Geochemical

326 rock standards BHVO-2 and NBS-688 were prepared using the same methods described above.
327 The amount of Fe^{2+} was measured on unheated samples using the Reichen and Fahey (1962)
328 procedure modified by including a titration of NBS-688 geochemical standard rock and
329 multiplying titrated sample FeO concentrations by the ratio of the titrated NBS-688 value to its
330 standard value (7.64 wt.% FeO; Govindaraju, K., 1994). The measurements and calculation
331 account for slight differences in acid concentrations and other vagaries in the technique.
332 Concentrations of Fe^{3+} were calculated using the XRF $\text{Fe}_2\text{O}_{3\text{total}}$, %LOI data, and the measured
333 Fe^{2+} values.

334 Samples were prepared and analyzed for trace elements using XRF. 7.0000 grams of each
335 sample were mixed with 1.4000 grams of high purity Copolywax powder and mixed for 10
336 minutes. The mixture was pressed into a briquette using a 50,000 psi press. Five dozen
337 geochemical rock standards were prepared using the above methods and were used to assemble
338 working curves for each element.

339 **3. Results and Discussion:**

340 3.1 Development of JSC-RN and final recipe

341 The base of JSC-RN was a mixture of two different size fractions of MMS that
342 approximated the <150 μm size fraction of Rocknest analyzed by both SAM and CheMin. Two
343 size fractions of MMS (dust and <2 mm) were mixed in various ratios and subsequently analyzed
344 for mean particle size using a Microtrac BlueWave laser particle size analyzer. A 65 wt.%
345 dust/35 wt.% < 2 mm MMS mixture was determined to have a particle size of approximately 90
346 % < 150 μm , which matches the particle size distribution of the Rocknest sample (Archer et al.
347 2014).

348 The MMS base (65 % dust, 35 % <2 mm) was augmented by adding phases to more
349 closely approximate the known mineralogy, evolved gases, and chemistry of Rocknest. The
350 highest priority was to replicate the 2.0 ± 1.3 wt. % (Archer et al., 2014) low temperature water
351 release (<450 °C) observed in the Rocknest soil sample. All potential additives and mixtures
352 were analyzed individually for their mineralogy and thermal and evolved gas profiles. Select
353 mixtures were analyzed for total chemistry using XRF.

354 Fifteen iterations of trial mixtures of MMS (65 % dust, 35 % <2 mm) and additives led to
355 the final recipe shown in Table 4, which most closely matched the evolved gases, water content,
356 total chemistry, and mineralogy of the Rocknest soil sample. Additives that were cost-effective,
357 pre-powdered, and available in large quantities were preferred. Each component, the reasoning
358 for adding it to the MMS base, and any processing steps prior to simulant mixing are described
359 below and in Table 4.

360 *Sodium perchlorate.*

361 Sodium perchlorate was added to the MMS base because it fairly closely reproduced the
362 mid temperature (~380 °C; Figure 1) O₂ release observed in SAM data from the Rocknest soil
363 sample. Although Na-, K-, and Ca perchlorate all evolve mid temperature O₂ without the
364 coevolution of HCl, Na perchlorate is less hygroscopic than other perchlorates and therefore
365 more feasible for large-scale production. Sodium perchlorate was added at 1 wt.% to
366 approximate the ClO₄ detected in Rocknest based on SAM mid temperature O₂ peak integrations.
367 Although ClO₄ was only detected at ~0.4 wt.% in Rocknest (Table 3), the actual amount of
368 perchlorate could be higher due to reactions with Fe-bearing phases and due to the oxidation of
369 reduced sulfur, both of which decrease the amount of evolved O₂ from perchlorate (Archer et al.,

370 2014). The sodium perchlorate arrived in granular form and was powdered with a ball mill prior
371 to mixing with the other simulant components.

372 *Sulfide and sulfate.*

373 Pyrite and ferric sulfate were added at 1 wt.% each to replicate the ~515 °C and 730 °C
374 SO₂ releases observed in Rocknest, respectively. As mentioned above, previous laboratory SAM-
375 like EGA experiments by McAdam et al. (2014) also supported the presence of iron sulfide and
376 sulfate in Rocknest. SO₃ abundances from SAM ranged from 0.5 ± 0.1 to 3.5 ± 0.7 wt.% in the
377 four runs of the Rocknest sample (Archer et al., 2014; Table 3), making 2 wt.% sulfur species in
378 JSC-RN a reasonable approximation. Pyrite was chosen as the reduced sulfide because, although
379 pyrrhotite is more likely to be present in martian samples (e.g., Lorand et al., 2005; Vaniman et
380 al., 2014), it oxidizes much more quickly than pyrite. Therefore, pyrite is more suitable for this
381 simulant because it is more stable over time. The pyrite arrived in hand-sample form and had to
382 be crushed and then powdered with a ball mill. The ferric sulfate was pre-powdered and no
383 additional processing steps were required prior to mixing with the other components.

384 *Granular ferric oxides.*

385 As stated previously, the Rocknest water release profile was broad enough that there were
386 likely multiple sources of water that contributed to the peak. Therefore, we selected multiple
387 materials that produced water release peaks spanning the temperature range of the Rocknest
388 water release. High capacity granular ferric oxide (GFO) was added because it evolved a broad
389 low temperature water release similar to what was observed in the Rocknest soil sample, and to
390 simulate the amorphous component in Rocknest. GFO's (both high and regular capacity) are
391 used in water filtration and large amounts can be purchased commercially at a relatively low

392 cost. Additionally, GFO's are pre-granulated, minimizing the steps for final simulant mixing and
393 homogenizing at the USGS. XRD of the high capacity GFO revealed two broad "humps" similar
394 to 2-line ferrihydrite with contributions from hematite (Supplementary figure 1). The high
395 capacity GFO simulated the nanophase iron oxides present in the amorphous component of
396 Rocknest (~35 wt.%; Table 1). Ferrihydrite is otherwise time-consuming to synthesize in the lab,
397 especially in the large-scale quantities necessary for ISRU experiments. The high capacity GFO
398 produced a water release peak (190 °C) lower than the Rocknest sample (280 °C), therefore it
399 could not be the only source of water in Rocknest.

400 Regular capacity GFO was added to the MMS base primarily because it produced a water
401 release peak at 245 °C, which was similar to the water release peak in the Rocknest soil sample
402 (280 °C). Regular capacity GFO was identified as goethite by XRD (Supplementary figure 2).
403 Goethite was not detected by CheMin in the Rocknest sample, but it can not be excluded because
404 it may have been present at or below the detection limit of the instrument (~1-2 wt. %) and/or
405 particle sizes were too small to coherently diffract X-rays. Both GFO's arrived as soft granules
406 and were powdered with a ball mill prior to mixing with the other simulant components.

407 *Goethite.*

408 Another goethite sample was added because it evolved a water peak at ~300 °C due to
409 dehydroxlation, which was slightly higher than the regular capacity GFO goethite (~245 °C) and
410 closer to the water release peak observed in Rocknest (280 °C). The addition of this goethite
411 served to broaden the overall H₂O release profile, making it more similar to what was observed
412 in Rocknest. Finely powdered goethite was sourced from a pottery pigment company (Table 4),
413 and also acted as an orange/yellow pigment for the final mixture. This goethite was pre-

414 powdered and no additional milling was required prior to mixing with the other simulant
 415 components.

416 *Forsterite*.

417 Forsterite, the Mg-rich endmember of olivine, was added to increase the total Mg and Si
 418 in the mixture. Forsterite did not produce any evolved gases within the SAM temperature range.
 419 Olivine was detected at 13.3 ± 4 wt.% in Rocknest, therefore the 10 wt.% added to JSC-RN was
 420 a reasonable approximation. The foresterite arrived in granular form and was powdered using a
 421 ball mill prior to mixing with other simulant components.

422

423 Table 4. Components of JSC-RN, their sources, the initial form they arrived in, and processing
 424 steps prior to mixing with other the components

Component	Wt. %	Source	Initial Form	Processing Steps
NaClO ₄	1	Synthetic, Sigma Aldrich	granules	Milling
Goethite	1.5	Laguna Clay Company	powder	None
Pyrite	1	Natural, Ward's	hand samples	Crushing, milling
Ferric Sulfate	1	Synthetic, Sigma Aldrich	powder	None
High Capacity GFO (ferrihydrite)	5	Kolar Filtration	granules	Milling
Regular capacity GFO (goethite)	2.5	Bayoxide	granules	Milling
Forsterite	10	Nature's Footprint	granules	Milling
Mojave Mars Simulant (65 % dust, 35 % <2 mm)	78	Jet Propulsion Laboratory	sand/dust	None

425

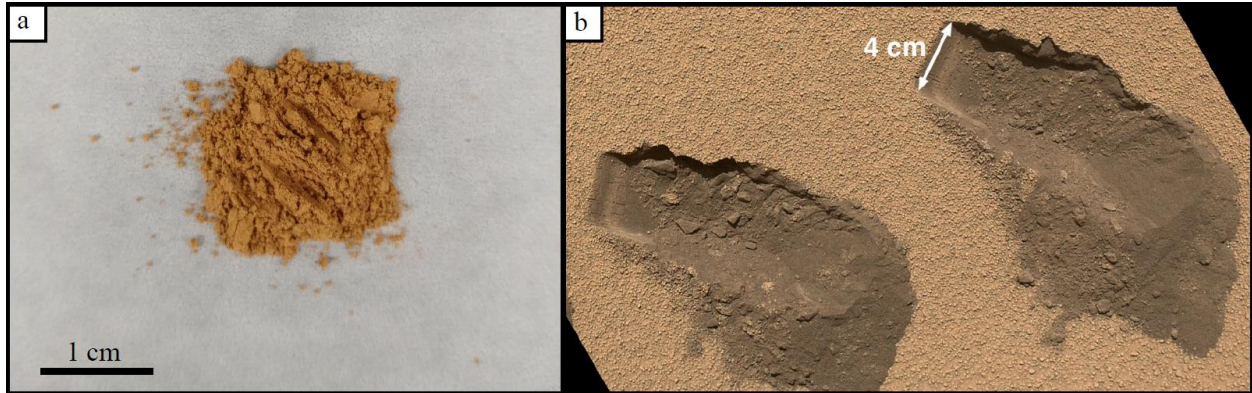
426

427 3.2 JSC-RN mixed by the USGS

428 The final recipe included the types and amounts of each additive and how to prepare (i.e.,
429 mill and mix) each additive (Table 4). This recipe, along with MMS dust, MMS <2 mm, and the
430 additives were sent to the Geology, Geophysics, and Geochemistry Science Center at the USGS
431 in Denver, CO for crushing, milling, and mixing. At the USGS, consolidated materials were
432 ground to fine powders using a 30 gallon ceramic lined ball mill with corundum grinding balls.
433 Consolidated materials were ground in ~50 kg aliquots for a total grinding time of 30 minutes.
434 All simulant components were mixed together in a 10 ft³ V-blender to ensure homogeneity.

435 Approximately 800 kg of JSC-RN were sent back to JSC from the USGS in 5-gallon
436 buckets (21 buckets total). Thirteen buckets of JSC-RN were randomly sampled and analyzed on
437 the TG/DSC/EGA instrument (described in section 2.1) and three of those samples were
438 analyzed with XRD (section 2.2). All 21 buckets of JSC-RN were subsampled and analyzed for
439 total chemistry using XRF (section 2.3). The results were analyzed for homogeneity between the
440 buckets and for any differences from the small prototype of JSC-RN made in the laboratory. The
441 results were also compared to Rocknest data from CheMin, SAM, and APXS. Images of JSC-RN
442 mixed by the USGS and the Rocknest sand shadow are shown in Figure 2.

443



444

445 Figure 2. a) JSC-RN simulant mixed by the USGS. b) Scoop trenches in the Rocknest sand
446 shadow, which were analyzed by instruments on the *Curiosity* rover.

447

448 3.3 Mineralogy and total chemistry of JSC-RN

449 The average quantitative mineralogy of three subsamples of JSC-RN mixed by the USGS
450 were mineralogically homogenous and better approximated the mineralogy of the Rocknest soil
451 sample compared to MMS (Table 1). The largest mineralogical differences between JSC-RN and
452 Rocknest analyzed by CheMin were pyroxene and the phyllosilicates, which were discrepancies
453 introduced by the MMS base (Table 1). JSC-RN better approximated the olivine abundance in
454 Rocknest compared to MMS alone (Table 1). JSC-RN was primarily developed to match the low
455 temperature evolved gases and the number of additives was minimized in order to make large-
456 scale production simpler and more cost-effective. Therefore, some differences in mineralogy
457 between JSC-RN and Rocknest analyzed by CheMin were expected.

458 The total chemistry of subsamples of JSC-RN prepared by the USGS indicated that they
459 were chemically homogenous and similar to Rocknest drill-fines that were analyzed by APXS
460 (Table 2). All oxides were similar between JSC-RN and Rocknest except for Al_2O_3 , which was

461 higher in JSC-RN due to the MMS base (13.7 wt.% in JSC-RN compared to 9.37 wt.% in
462 Rocknest; Table 2). This was expected because terrestrial basalts are known to contain more Al
463 than martian basalts (e.g., Wänke & Dreibus, 1988; McSween et al., 2009). Overall, JSC-RN
464 was a better chemical match to Rocknest analyzed by APXS compared to MMS alone.

465 3.4 Thermal and evolved gas analysis of JSC-RN

466 Evolved gas analysis of the 13 subsamples of JSC-RN mixed by the USGS demonstrated
467 that they were homogenous and matched low temperature (<450 °C) gas evolutions detected by
468 SAM in Rocknest (Figure 1). Low temperature (<450 °C) weight loss due to evolved water in the
469 JSC-RN subsamples was consistently ~2 wt.% (Figure 1), which was similar to H₂O abundances
470 from Rocknest as detected by SAM (2.0 ± 1.3 wt. %; Archer et al., 2014; Table 3). JSC-RN
471 evolved minor amounts of water >450 °C due to phyllosilicate dehydroxylation, which was not
472 consistent with results from SAM. The O₂ release peak from JSC-RN was slightly lower (312
473 °C) than that of Rocknest (380 °C), possibly due to differences in the type of oxychlorine and/or
474 effects of Fe-bearing minerals in the sample. The lower temperature SO₂ release in JSC-RN was
475 the same as Rocknest analyzed by SAM (both ~515 °C). However, the second SO₂ peak in
476 Rocknest (~730 °C) was lower than that of JSC-RN (~810 °C). The discrepancy in the second
477 SO₂ release could be caused by differences in the cation-type of sulfate and/or effects of other
478 phases in the sample on sulfate decomposition temperature. The high temperature (>600 °C) HCl
479 release present in the small-batch prototype of JSC-RN prepared in the laboratory and in
480 Rocknest analyzed by SAM was not present in the JSC-RN subsamples mixed by the USGS
481 (Figure 1). It is currently unknown what caused the discrepancy in the high temperature HCl
482 evolutions between the USGS-prepared and small lab-prepared prototype of JSC-RN, but high-
483 temperature HCl was not a priority for testing the ISRU water-extraction equipment. Overall,

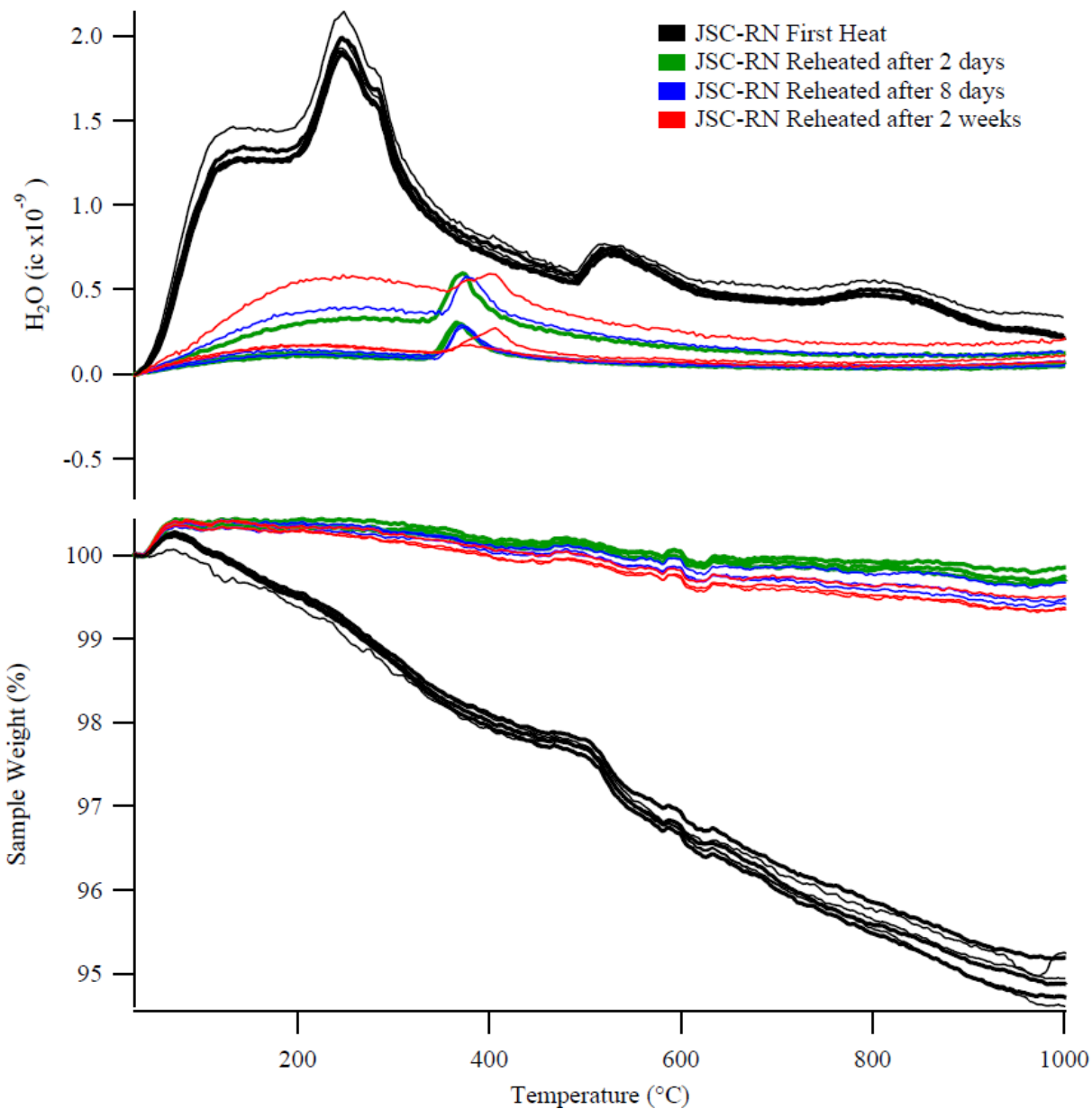
484 JSC-RN broadly matched the SO₂, O₂, and H₂O gas evolutions detected by SAM in the Rocknest
485 soil sample and was a much better match than the MMS mixture without additives (Figure 1).
486 Specifically, JSC-RN matched the low temperature water profiles and abundances as detected by
487 SAM in the Rocknest soil sample.

488 3.5 Water re-adsorption in JSC-RN

489 JSC-RN mixed by the USGS was analyzed for its ability to re-adsorb atmospheric water
490 after being heated in order to determine if previously heated samples could be reused for water
491 extraction purposes. Nine sub-sample of JSC-RN were heated to 1000 °C in a Labsys EVO
492 DSC/TG/mass spectrometer using the methods described in section 2.1 and allowed to cool to
493 room temperature. The samples were left exposed to laboratory air for 2 days, 8 days, and 2
494 weeks (3 of each). The same samples were then re-heated to 1000 °C on the Labsys EVO. TG
495 weight loss data from the first heat and second heat analyses were compared in order to
496 determine how much water was re-adsorbed by the post-heat sample when left exposed to
497 laboratory air.

498 Results from the water re-adsorption experiments demonstrated that JSC-RN did not re-
499 adsorb water after being heated to 1000 °C and then exposed to laboratory air for 2 days, 5 days,
500 and 2 weeks. When heated to 1000 °C for the first time, JSC-RN had a TG weight-loss of ~2
501 wt.%, most of which was due to water (Figure 3). When the same sample was reheated to 1000
502 °C after being exposed to laboratory air for 2 days-2 weeks, it had a TG weight-loss of <0.1
503 wt.% at 450 °C (Figure 3). The low amount of water re-adsorption indicates that JSC-RN cannot
504 be reused for water-extraction purposes after it is heated. This was expected because the low
505 temperature water release in JSC-RN was not solely due to adsorbed water; it also had

506 contributions from structural water and hydroxylated phases (e.g., goethite) that decomposed
507 during thermal analysis.



508
509 Figure 3. H₂O and sample weight loss from JSC-RN produced by the USGS after being heated to
510 1000 °C (first heat), and then reheated to 1000 °C after the sample was exposed to laboratory air
511 for 2 days, 8 days, and 2 weeks.

512 3.6 Applications of JSC-RN

513 JSC-RN is ideal for large-scale experiments and device testing where volatile content is
514 the primary focus. This includes the testing of equipment meant to evolve gases through heating
515 for uses such as liquid H₂O for human consumption, breathable O₂, or rocket propellant. JSC-RN
516 is the highest fidelity martian soil simulant available in terms of evolved O₂, SO₂, and
517 particularly the low temperature (<450 °C) H₂O.

518 JSC-RN is suitable for most other experiments and equipment testing where large
519 quantities of martian soil simulant are necessary. JSC-RN is feasible and cost-effective to make
520 in large quantities because it uses commercially available additives, most of which are pre-
521 granulated or powdered. Large-scale applications for JSC-RN include ISRU systems and
522 component testing, ISRU plant growth studies, and ISRU habitat studies.

523 JSC-RN can also be used for geophysical applications where a crushed-rock based
524 simulant is preferred. Crushed-rock simulants are ideal for testing ISRU technologies where
525 geophysical properties are important (e.g., rover wheel testing) (Peters et al., 2008). Although
526 both JSC-RN and the original MMS simulant are crushed-rock based simulants, JSC-RN is a
527 closer match to Rocknest in terms of mineralogy, chemistry, and evolved gases. Mineral-based
528 simulants such as MGS-1 are more applicable for studies that require mineralogy that precisely
529 matches the quantified mineralogy of martian soils. Applications that may require a mineral-
530 based simulant include science research that focuses on mineralogy, such as mineral alteration
531 experiments.

532

533

534 3.7 Future development of JSC-RN

535 JSC-RN will be further developed by changing the base from MMS to a crushed rock that
536 better simulates martian soil mineralogy. The mineralogy of MMS reported by Peters et al.
537 (2008) and the mineralogy of MMS sent to JSC were different. One of the major differences was
538 that the batches of MMS sent to JSC contained phyllosilicates (Table 1). The presence of
539 phyllosilicates in MMS caused high temperature (>450 °C) water releases in JSC-RN, which
540 were not observed in Rocknest (Figure 1). Additionally, MMS dust and MMS <2 mm did not
541 contain olivine as reported in Peters et al. (2008). Several active basalt quarries are currently
542 being evaluated for their potential to be mined for large quantities of crushed rock-based martian
543 soil simulant which better matches the mineralogy of Rocknest.

544 It is important to note that the future development of JSC-RN is highly dependent on the
545 user's application and therefore, what properties (e.g., mineralogy, chemistry) are important. For
546 example, if JSC-RN were to be used for mineral alteration studies, it should be modified to more
547 closely match the mineralogy of Rocknest. If the high temperature (>450 °C) evolved gases (e.g.,
548 SO₂, HCl) are important for the simulant application, it should be modified to more closely
549 match the high temperature evolved gases from Rocknest. Overall, future development of JSC-
550 RN will reflect the needs of the simulant-using community.

551

552 **Conclusions**

553 JSC-RN was designed to mimic the evolved gases, mineralogy, and total chemistry of the
554 well-characterized martian soil sample, Rocknest, which was analyzed by the *Curiosity* rover in
555 Gale Crater, Mars. JSC-RN was specifically developed for use in large-scale ISRU systems and

556 component testing of a water-extraction device where the low temperature (<450 °C) evolved
557 gases were of primary importance. JSC-RN was homogenous and similar to Rocknest in terms of
558 mineralogy, total chemistry, and low temperature evolved gases. Specifically, the water content
559 of JSC-RN was ~2 wt. %, which was similar to H₂O abundances from Rocknest as detected by
560 SAM. JSC-RN is an ideal martian soil simulant for use in studies that require large quantities of
561 low-cost martian soil simulant, in particular studies where volatile content is of primary
562 importance. However, we stress that further modifications to the JSC-RN will depend on the
563 user's application (e.g., water extraction, geotechnical tests).

564

565 **Acknowledgements:**

566 We thank Steve Wilson and the staff at the Geology, Geophysics, and Geochemistry
567 Science Center at the USGS in Denver, CO for processing and mixing large-scale batches of
568 JSC-RN. We thank Greg Peters and the processing lab at JPL for providing the MMS <2 mm
569 and MMS dust. We thank S.J. Ralston for providing edits and feedback on this paper prior to
570 submission. Mertzman thanks the NSF-MRI Program for XRF Instrumentation support (NSF-
571 EAR 1872311) and Karen R. Mertzman for her ongoing meticulous work in the lab. We
572 acknowledge Kevin Cannon and the University of Central Florida simulant lab for providing
573 information on simulants on their publicly available website
574 (<https://sciences.ucf.edu/class/planetary-simulant-database/>).

575

576

577

578 **Data statement:**

579 Data published in this paper are publicly available on the Harvard Dataverse data
580 repository: <https://doi.org/10.7910/DVN/7BH7NL>

581

582 **References:**

583 Achilles, C.N., Downs, R.T., Ming, D.W., Rampe, E.B., Morris, R.V., Treiman, A.H., Morrison,
584 S.M., Blake, D.F., et al. (2017). Mineralogy of an active eolian sediment from the Namib dune,
585 Gale crater, Mars. *Journal of Geophysical Research: Planets*. 122, 2344-2361, doi:
586 10.1002/2017JE005262.

587

588 Allen, C.C., Jager, K.M., Morris, R.V., Lindstrom, D.J., Lindstrom, M. M., Lockwood, J.P.
589 (1998). Martian soil simulant available for scientific, educational study. *Eos, Transactions*
590 *American Geophysical Union*. 79, 405-412.

591

592 Archer, P.D., Franz, H.B., Sutter, B., Arevalo, R.D., Coll, P., Eigenbrode, J.L., Glavin, D.P.,
593 Jones, J.J., et al. (2014). Abundances and implications of volatile-bearing species from evolved
594 gas analysis of the Rocknest aeolian deposit, Gale Crater, Mars. *Journal of Geophysical*
595 *Research: Planets*. 119, 237-254, doi:10.1002/2013JE004493.

596

597 Biemann, K., Oro, J., Toulmin III, P., Orgel, L.E., Nier, A.O., Anderson, D.M., Simmonds, P.G.,
598 Flory, D., et al. (1977). The search for organic substances and inorganic volatile compounds in
599 the surface of Mars, *Journal of Geophysical Research*. 82, 4641–4658.

600

601 Bish, D.L., Blake, D.F., Vaniman, D.T., Chipera, S.J., Morris, R.V., Ming, D.W., Treiman, A.H.,
602 Sarrazin, P., et al. (2013). X-ray diffraction results from Mars Science Laboratory: mineralogy of
603 Rocknest at Gale Crater. *Science*, 341, 1-6.

604

605 Bish, D.L. & Howard, S.A. (1988). Quantitative phase analysis using the Rietveld method.
606 *Journal of Applied Crystallography*. 21, 86-91.

607

608 Blake, D.F., Morris, R.V., Kocurek, G., Morrison, S.M., Downs, R.T., Bish, D., Ming, D.W.,
609 Edgett, K.S., et al. (2013). Curiosity at Gale Crater, Mars: characterization and analysis of the
610 Rocknest sand shadow. *Science*. 341.

611

612 Cannon, K.M., Britt, D.T., Smith, T.M., Fritsche, R.F., Batchelder, D. (2019). Mars global
613 simulant MGS-1: A Rocknest-based open standard for basaltic martian regolith simulants.
614 *Icarus*. 317, 470-478.

615

616 Clark, J.V., Sutter, B., McAdam, A.C., Rampe, E.B., Archer, P.D., Ming, D.W., Navarro-
617 Gonzalez, R., Mahaffy, P., Lapen, T.J. (2020). High-temperature HCl evolutions from mixtures

618 of perchlorates and chlorides with water-bearing phases: Implications for the Sample Analysis at
619 Mars (SAM) instrument in Gale crater, Mars. *Journal of Geophysical Research: Planets*. 125,
620 doi: 10.1029/2019JE006173.

621 Evans, D.L. & Adams, J.B. (1979). Comparison of Viking Lander multispectral images and
622 laboratory reflectance spectra of terrestrial samples. *Lunar and Planetary Science Conference*.
623 Houston, TX.

624

625 Freissinet, C., Glavin, D.P., Mahaffy, P.R., Miller, K.E., Eigenbrode, J.L., Summons, R.E., et al.
626 (2015). Organic molecules in the Sheedpbed Mudstone, Gale Crater, Mars. *Journal of*
627 *Geophysical Research Planets*. 120, 495-514, doi: 10.1002/2014JE004737

628

629 Golden, C.D., Ming, D.W., Sutter, B., Clark, B.C., Morris, R.V., Boynton, W., Hecht, M.,
630 Kounaves, S. (2009). Sulfur Mineralogy at the Mars Phoenix Landing Site. *Lunar and Planetary*
631 *Science Conference*. The Woodlands, TX.

632

633 Govindaraju, K. (1994). Compilation of Working Values and Sample Description for 383
634 Geochemical standards. *Geostandards Newsletter*. 18, 1-58.

635

636

637 Hamilton, V.E., McSween, H.Y., Hapke, B. (2005). Mineralogy of martian atmospheric dust
638 inferred from thermal infrared spectra of aerosols. *Journal of Geophysical Research*. 110,
639 E12006, doi: 10.1029/2005JE002501.

640

641 Hecht, M.H., Kounaves, S.P., Quinn, R.C., West, S.J., Young, S.M.M., Ming, D.W., Clark, B.C.,
642 Boynton, W.V., Hoffman, J., DeFlores, L.P., Goispodinova, K., Kapit, J., Smith, P.H. (2009).
643 Detection of perchlorate and the soluble chemistry of Martian soil at the Phoenix Lander site.
644 *Science*. 325.

645

646 Hogancamp, J.V., Sutter, B., Morris, R.V., Archer, P.D., Ming, D.W., Rampe, E.B., Mahaffy, P.,
647 Navarro-Gonzalez, R. (2018). Chlorate/Fe-Bearing Phase Mixtures as a Possible Source of
648 Oxygen and Chlorine Detected by the Sample Analysis at Mars Instrument in Gale Crater, Mars.
649 *Journal of Geophysical Research: Planets*, doi: 10.1029/2018JE005691.

650

651 Leshin, L.A., Mahaffy, P.R., Webster, C.R., Cabane, M., Coll, P., Conrad, P.G., Archer, P.D.,
652 Atreya, S.K., et al. (2013). Volatile, isotope, and organic analysis of martian fines with the Mars
653 Curiosity rover. *Science*. 341.

654

655 Lorand, J.-P., Chevrier, V., Sautter, V. (2005), Sulfide mineralogy and redox conditions in some
656 shergottites, *Meteoritics and Planetary Science*. 40, 1257–1272.

657

658 Mahaffy, P., Webster, C. R., Cabane, M., Conrad, P., Coll, P., Atreya, S. K., et al. (2012). The
659 Sample Analysis at Mars Investigation and Instrument Suite. *Space Science Reviews*. 170, 401-
660 478, doi: 10.1007/s11214-012-9879-z.

661

662 McAdam, A.C., Franz, H.B., Sutter, B., Archer, P.D., Freissinet, C., Eigenbrode, J.L., Ming,
663 D.W., Atreya, S.K., Bish, D.L., Blake, D.F., Bower, H.E., Brunner, A., Buch, A., Glavin, D.P.,
664 Grotzinger, J.P., Mahaffy, P.R., McLennan, S.M., Morris, R.V., Navarro-Gonzalez, R., Rampe,
665 E.B., Squyres, S.W., Steele, A., Stern, J.C., Sumner, D.Y., Wray, J.J. (2014). Sulfur-bearing
666 phases detected by evolved gas analysis of the Rocknest aeolian deposit, Gale Crater, Mars.
667 *Journal of Geophysical Research-Planets*. 119, 373-393, doi:10.1002/2013JE004518.

668

669 McSween, H.Y., Taylor, G.J., Wyatt, M.B. (2009). Elemental composition of the martian crust.
670 *Science*. 324.

671

672 Ming, D.W. & Morris, R.V. (2017). Chemical, mineralogical, and physical properties of martian
673 dust and soil. *Dust in the Atmosphere of Mars and Its Impact on Human Exploration Workshop*.
674 Houston, TX.

675

676 Morris, R.V., Golden, D.C., Bell, J.F., Lauer, H.V., Adams, J.B. (1993). Pigmenting agents in
677 martian soils—Inferences from spectral, Mossbauer, and magnetic-properties of nanophase and

678 other iron-oxides in Hawaiian Palagonitic Soil Pn-9. *Geochimica et Cosmochimica Acta*. 57,
679 4597-4609.

680

681 Morris, R.V., Golden, D.C., Bell III, J.F., Shelfer, T.D., Scheinost, A.C., Hinman, N.W., Furniss,
682 G., Mertzman, S.A., et al. (2000). Mineralogy, composition, and alteration of Mars Pathfinder
683 rocks and soils' Evidence from multispectral, elemental, and magnetic data on terrestrial
684 analogue, SNC meteorite, and Pathfinder samples. *Journal of Geophysical Research*. 105, 1757-
685 1817.

686

687 Morrison, S.M., Downs, R.T., Blake, D.F., Prabhu, A., Eleish, A., Vaniman, D.T., Ming, D.W.,
688 Rampe, E.B. (2018a). Relationships between unit-cell parameters and composition for rock-
689 forming minerals on Earth, Mars, and other extraterrestrial bodies. *American Mineralogist*. 103,
690 doi: 10.2138/am-2018-6123.

691

692 Morrison, S.M., Downs, R.T., Blake, D.F., Vaniman, D.T., Ming, D.W., Hazen, R.M., Treiman,
693 A.H., Achilles, C.N. (2018b). Crystal chemistry of martian minerals from Bradbury Landing
694 through Naukluft Plateau, Gale crater, Mars. *American Mineralogist*. 103, 857-871, doi:
695 10.2138/am-2018-6124.

696

697 Peters, G.H., Abbey, W., Bearman, G.H., Mungas, G.S., Smith, J.A., Anderson, R.C., Douglas,
698 S., Beegle, L.W. (2008). Mojave Mars simulant – characterization of a new geologic Mars
699 analog. *Icarus*. 197, 470-479.

700

701 Reichen, L.E. and Fahey, J.J. (1962). An Improved Method for the Determination of FeO in
702 Rocks and Minerals Including Garnet. U.S. Geological Survey Bulletin 1144B, 1-5.

703

704 Smith, M.D. (2009). THEMIS observations of Mars aerosol optical depth from 2002-2008.
705 *Icarus*. 202, 444-452.

706

707 Sutter, B., McAdam, A. C., Mahaffy, P. R., Ming, D. W., Edgett, K. S., Eigenbrode, J. L., et al.
708 (2017). Evolved gas analyses of sedimentary rocks and eolian sediment in Gale Crater, Mars:
709 Results of the Curiosity rover’s sample analysis at Mars instrument from Yellowknife Bay to the
710 Namib Dune. *Journal of Geophysical Research: Planets*. 122, 2574–2609, doi:
711 10.1002/2016JE005225.

712

713 Vaniman, D.T., Bish, D.L., Ming, D.W., Bristow, T.F., Morris, R.V., Blake, D.F., Chipera, S.J.,
714 Morrison, S.M. (2014). Mineralogy of a mudstone at Yellowknife Bay, Gale Crater, Mars.
715 *Science*. 343, doi: 10.1126/science.1243480.

716

717 Wänke, H. & Dreibus, G. (1988). Chemical composition and accretion history of terrestrial
718 planets. *Philosophical Transactions of the Royal Society A*. 325, doi: 10.1098/rsta.1988.0067.

719

720 Webster, C.R., Mahaffy, P.R., Flesch, G.J., Niles, P.B., Jones, J.H., Leshin, L.A., et al. (2013).
721 Isotope Ratios of H, C, and O in CO₂ and H₂O of the Martian Atmosphere. *Science*. 341, 260-
722 263, doi: 10.1126/science.1237961.

723

724 Yen, A.S., Gellert, R., Schroder, C., Morris, R.V., Bell III, J.F., Knudson, A.T., Clark, B.C.,
725 Ming, D.W., et al. (2005). An integrated view of the chemistry and mineralogy of martian soils.
726 *Nature*. 436, 49-54, doi:10.1038/nature03637.